Tonotopic Organization of Vertical Cells in the Dorsal Cochlear Nucleus of the CBA/J Mouse

Michael A. Muniak,[1,2]* and David K. Ryugo[1,2,3,4]

[1]Department of Neuroscience, Johns Hopkins University, Baltimore, Maryland 21205
[2]Hearing Research Program, Garvan Institute of Medical Research, Sydney, New South Wales 2010, Australia
[3]Deparment of Otolaryngology-Head and Neck Surgery, Johns Hopkins University, Baltimore, Maryland 21205
[4]School of Medical Sciences, University of New South Wales, Sydney, New South Wales 2052, Australia

ABSTRACT

The systematic and topographic representation of frequency is a first principle of organization throughout the auditory system. The dorsal cochlear nucleus (DCN) receives direct tonotopic projections from the auditory nerve (AN) as well as secondary and descending projections from other sources. Among the recipients of AN input in the DCN are vertical cells (also called tuberculoventral cells), glycinergic interneurons thought to provide on- or near-best-frequency feed-forward inhibition to principal cells in the DCN and various cells in the anteroventral cochlear nucleus (AVCN). Differing lines of physiological and anatomical evidence suggest that vertical cells and their projections are organized with respect to frequency, but this has not been conclusively demonstrated in the intact mammalian brain. To address this issue, we retrogradely labeled vertical cells via physiologically targeted injections in the AVCN of the CBA/J mouse. Results from multiple cases were merged with a normalized 3D template of the cochlear nucleus (Muniak et al. [2013] J. Comp. Neurol. 521:1510–1532) to demonstrate quantitatively that the arrangement of vertical cells is tonotopic and aligned to the innervation pattern of the AN. These results suggest that vertical cells are well positioned for providing immediate, frequency-specific inhibition onto cells of the DCN and AVCN to facilitate spectral processing. J. Comp. Neurol. 522:937–949, 2014.

INDEXING TERMS: 3D reconstruction; auditory nerve; frequency organization; interneuron; tuberculoventral; type II

The dorsal cochlear nucleus (DCN) receives direct projections from the auditory nerve (AN) and is thought to play a vital role in spectral feature processing and sound localization (Young and Oertel, 2003). This primary auditory input is strictly organized by frequency (Fekete et al., 1984; Ryugo and May, 1993; Muniak et al., 2013), whereas secondary projections represent multiple different modalities that include ascending somatosensory, vestibular, and reticular inputs (Itoh et al., 1987; Weinberg and Rustioni, 1987; Burian and Gstoettner, 1988; Young et al., 1995; Wright and Ryugo, 1996; Kanold and Young, 2001; Ohlrogge et al., 2001; Haenggeli et al., 2005; Zhan and Ryugo, 2007) as well as descending projections from auditory cortex (Weedman and Ryugo, 1996; Meltzer and Ryugo, 2006) and the inferior colliculus (Caicedo and Herbert, 1993; Malmierca et al., 1996). The DCN of mammals is a layered structure containing a number of identifiable cell types, each with unique morphology (Osen, 1969; Brawer et al., 1974; Lorente de Nó, 1981; Webster and Trune, 1982), response properties (Evans and Nelson, 1973; Young and Brownell, 1976; Davis et al., 1996; Ma and Brenowitz, 2012), and ascending connections (Osen, 1972; Ryugo et al., 1981; Malmierca et al., 2002). Among these are local circuit interneurons called *vertical cells* (Lorente de Nó, 1981).

Additional Supporting Information may be found in the online version of this article.

Grant sponsor: National Institutes of Health/National Institute on Deafness and Other Communication Disorders (NIDCD); Grant number: DC00023; Grant number: DC00143; Grant number: DC00232; Grant number: DC04395; Grant number: DC05211; Grant number: DC05909; Grant sponsor: National Health and Medical Research Council (NHMRC) of Australia; Grant number: 1009482; Grant sponsor: Garnett Passe and Rodney Williams Memorial Foundation; Grant sponsor: Fairfax Foundation; Grant sponsor: Life Science Research Award from the New South Wales Office of Science and Medical Research.

*CORRESPONDENCE TO: Michael A. Muniak, Hearing Research Program, Garvan Institute of Medical Research, 384 Victoria Street, Sydney, New South Wales 2010, Australia. E-mail: m.muniak@garvan.org.au

Received May 20, 2013; Revised July 30, 2013;
Accepted August 16, 2013.
DOI 10.1002/cne.23454
Published online August 24, 2013 in Wiley Online Library (wileyonlinelibrary.com)

Vertical cells, also named *tuberculoventral cells*, reside within the deep layer of the DCN and have small, elongate cell bodies (Lorente de Nó, 1981). They are glycinergic (Wenthold, 1987; Saint Marie et al., 1991; Wickesberg et al., 1994) and exhibit smooth dendritic trees that are oriented within the plane of an isofrequency sheet along with their locally terminating axonal collaterals (Osen, 1983; Zhang and Oertel, 1993). Vertical cells are the presumed source of the type II electrophysiological response in the DCN, characterized as having a "V"-shaped excitatory area flanked by inhibitory sidebands, low rates of spontaneous activity, nonmonotonic rate-level functions, poor responses to broadband noise stimuli, and robust responses to tones near their best frequency (BF; Evans and Nelson, 1973; Young and Brownell, 1976; Young and Voigt, 1982; Davis et al., 1996; Spirou et al., 1999; Rhode, 1999). There is strong evidence to suggest that type II neurons provide feed-forward inhibition to principal cells of the DCN, partially shaping their type IV response (Voigt and Young, 1980, 1990; Nelken and Young, 1994; Spirou et al., 1999; Davis and Young, 2000). Indeed, functional synapses between vertical cells and pyramidal cells (a type of principal cell) have recently been demonstrated (Kuo et al., 2012).

Vertical cells are known to send projections to the anteroventral cochlear nucleus (AVCN; Young, 1980; Feng and Vater, 1985; Wickesberg and Oertel, 1988; Saint Marie et al., 1991; Zhang and Oertel, 1993) via the tuberculoventral tract (Lorente de Nó, 1981), providing a source of inhibitory signaling to bushy and stellate cells in the AVCN (Wickesberg and Oertel, 1990). Physiological evidence suggests that inhibition on these AVCN cells arrives from cells at or near the same BF (Caspary et al., 1994), although the source of this inhibition has not been conclusively demonstrated. Furthermore, anatomical studies in slice preparations have shown that vertical cells receive the same AN input as the cells in the AVCN to which they are targeting (Wickesberg and Oertel, 1988). Collectively, these indirect lines of evidence imply that vertical cells of the DCN are tonotopically organized. There is, however, scant direct evidence to support this conclusion in the intact mammalian brain (Feng and Vater, 1985). To investigate this idea, we labeled vertical cells via physiologically targeted injections in the AVCN and demonstrate, by merging the results of multiple experimental cases to a single model (Muniak et al., 2013), that their arrangement is tonotopic in three dimensions. In addition, comparisons are made with a quantitative model of frequency representation in the cochlear nucleus (CN; Muniak et al., 2013) to show that this tonotopic arrangement is well aligned to the cochleotopic organization of the DCN.

Abbreviations

AN	auditory nerve
AVCN	anteroventral cochlear nuclues
BF	best frequency
CN	cochlear nucleus
DCN	dorsal cochlear nucleus
MRA	multiple regression analysis
PVCN	posteroventral cochlear nucleus
VCN	ventral cochlear nucleus

MATERIALS AND METHODS

Animals

Twenty-one adult CBA/J mice (2 male, 19 female; Jackson Laboratories, Bar Harbor, ME) were used in this study. Mice ranged in age from 2.5 to 4 months (mean 12 $\pm$ 1.3 weeks) and weighed between 17 and 30 g (mean 23.4 $\pm$ 3.6 g). Other results from these animals have been reported elsewhere (Muniak et al., 2013). All procedures were in accordance with National Institutes of Health (NIH) guidelines and were approved by the Animal Care and Use Committee of the Johns Hopkins University School of Medicine. All data are reported as mean $\pm$ standard deviation (SD).

Surgery

Mice were prepared for recordings using aseptic surgical techniques. Anesthesia was induced via an intraperitoneal (IP) injection containing a mixture of ketamine (100 mg/kg), xylazine (10 mg/kg), and 14.25% ethanol. Atropine (0.1–0.2 mg/kg, intramuscularly [IM]) and dexamethasone (0.6 mg/kg, IM) were administered to reduce oral secretions and brain swelling, respectively. When the animal was areflexic, it was secured in a stereotaxic frame (Stoelting, Wood Dale, IL). Body temperature was maintained at 37°C with a temperature-feedback-controlled heating pad. Through a midline incision, a craniotomy overlying the inferior colliculus was made 2 mm lateral and 2 mm caudal to lambda, after which the dura was opened. Upon conclusion of the experiment, gelfoam was placed over the skull opening and the soft tissue pulled back up and closed with nylon sutures. Postsurgical treatment included a topical antibiotic and administration of lactated Ringer's ($\sim$0.25 ml, IP), doxapram (10 mg/kg, IM) to stimulate respiration, and butorphanol (5 mg/kg, subcutaneous) for postsurgical analgesia.

Electrophysiology

Recordings were carried out in a heated, double-walled, sound-attenuated chamber (IAC, Bronx, NY). Custom MatLab (Mathworks, Natick, MA) routines were used for stimulus delivery and neural recording.

Acoustic stimuli were generated by manually adjusting an analog test oscillator during search (4200B; Krohn-Hite, Brockton, MA) or via computer-controlled hardware (RP2, SM5; Tucker-Davis Technologies [TDT], Alachua, FL). Signals were amplified (D-75A; Crown, Elkhart, IN), attenuated (PA5; TDT), and delivered by a calibrated free-field speaker (40-5036 or Super Tweeter; Radio Shack, Fort Worth, TX) placed directly in front of the animal.

Single- and multiunit recordings were performed with glass micropipettes (1.2 mm outer diameter) containing fluorescein dextran (MW 10,000; D-1820; Molecular Probes/Invitrogen, Carlsbad, CA) or tetramethylrhodamine dextran (MW 10,000; D-1817; Molecular Probes), each diluted to 10% w/v in a solution of 0.5 M Tris buffer, pH 7.6, and 3 M NaCl. The inner diameter of the pipette tip was 10 μm, and the pipettes had 2–4-MΩ impedances. Signals were amplified (1800; A-M Systems, Carlsborg, WA), filtered (3202; Krohn-Hite), and digitized for analysis (PCI-6602; National Instruments, Austin, TX).

Broadband noise or sinusoidal tone bursts (200 msec duration, 5 msec rise/fall) were delivered as the recording electrode was advanced into the brain using a motorized hydraulic micromanipulator (650; Kopf Instruments, Tujunga, CA). A 16° posterior angle was used to approach the CN, guided by atlas coordinates (Franklin and Paxinos, 1997). Arrival into the nucleus was heralded by the presence of sound-evoked spike discharges. BF and threshold were estimated audiovisually and then confirmed using an automated tuning curve protocol that measured responses to a four-octave (oct.) frequency sweep centered on the test frequency at 20 dB above threshold, sampling every 1/25 oct. At selected locations, fluorescent dextran tracer was injected iontophoretically using a high-voltage, constant-current source (CS 3; Midgard/Stoelting) set at 5 μA of positive current (50% duty cycle) for 6–10 minutes. The pipette remained in position for 5 minutes before being withdrawn. An injection at a second frequency region in the CN using a different fluorescent tracer was attempted in most animals.

Preparation of tissue for microscopy

Two weeks following dye injection, animals were deeply anesthetized with a lethal dose of sodium pentobarbital (100 mg/kg, IP) and perfused transcardially with 3% paraformaldehyde in 0.1 M phosphate buffer, pH 7.3. The brainstem was dissected from the skull and post-fixed overnight in the 3% paraformaldehyde solution. On the next day, it was embedded in gelatin-albumin hardened with 4% paraformaldehyde, cut in the transverse plane using a vibrating microtome (Vibratome, Bannockburn, IL) at 50 μm thickness, mounted, and coverslipped in Krystalon (Harleco, Philadelphia, PA).

CN reconstruction

Brain sections were photographed and reconstructed following methods described previously (Muniak et al., 2013). Briefly, serial-section digital light micrographs were collected and registered along the anterior–posterior axis in Photoshop (Adobe Systems, San Jose, CA) and exported to Amira (Visage Imaging, San Diego, CA), where the CN border was outlined with a graphics tablet (Cintiq 12WX; Wacom, Vancouver, WA). This collection of outlines was used to generate a 3D surface of the CN. Cases were normalized by independently aligning each surface to a template CN surface (Muniak et al., 2013) using an iterative routine in Amira that produced an affine transformation matrix. All imported image data from a single animal were confined to the same bounding box so that the transformation matrix was consistent across that case.

Vertical cell analysis

Fluorescent micrographs were taken alongside bright-field micrographs and subjected to alignment and export manipulations in Photoshop identical to those described above. Images were collected using appropriate filter sets for red (rhodamine) and green (fluorescein) wavelength emissions and stored in separate color channels of a document, even if only one injection was made. This procedure facilitated the extraction of labeled features from endogenous background signals that appeared in both channels. In some cases, level adjustments and color enhancements were applied to bring out weak signals and to balance the overall amount of background signal across channels. Because our analysis focused on the location of labeled pixels but not pixel luminance, these manipulations did not alter our findings.

Micrographs were imported into Neurolucida (MicroBrightField, Williston, VT) to identify the locations of retrogradely labeled cells in the DCN. The location of each cell was registered with respect to its x-, y-, and z-coordinates and exported to MatLab for analysis. Cell coordinates were normalized by applying the transformation matrix, and their spatial representation was visualized in 3D by generating small, uniformly sized spheres.

RESULTS

Electrophysiology

In total 26 recording sites were characterized. BFs ranged from 6.2 to 56 kHz, with thresholds ranging from 8.6 to 37.6 dB SPL (Table 1). Iontophoretic tracer injections were made at each recording site.

TABLE 1.
Frequency Tuning and Vertical Cell Counts for All Cases

Mouse ID/ injection	Frequency (kHz)	Threshold (dB SPL)	Vertical cell count
22-Fluo	22.1	8.8	24
23-Fluo	8.7	15.0	79
25-Fluo	9.5	17.8	49
27-Fluo	56.0	15.1	30
30-Fluo	9.1	20.3	43
30-Rhod	11.3	21.2	96
31-Rhod	33.7	21.2	26
32-Fluo	41.7	18.7	13
33-Rhod	25.0	16.2	112
35-Fluo	33.0	22.5	16
36-Fluo	34.5	8.6	18
36-Rhod	20.7	13.2	63
37-Rhod	49.0	30.0	12
38-Rhod	10.0	23.9	128
38-Fluo	17.7	17.8	73
39-Rhod	13.8	18.1	87
40-Rhod	6.8	24.9	39
42-Fluo	6.2	33.1	70
45-Rhod	27.0	37.6	20
45-Fluo	48.5	10.2	16
49-Fluo	28.6	24.6	47
51-Rhod	43.3	23.7	33
52-Rhod	33.4	24.5	62
55-Rhod	12.8	24.7	71
55-Fluo	19.5	29.9	11
56-Fluo	25.3	29.9	21

Retrogradely labeled vertical cells

All recordings and injections were confined to the AVCN and produced discrete deposits (Fig. 1). Injection sites were characterized by a dense accumulation of dye that varied from approximately 50 to 400 μm in width. Fibers emanate away from the injection site in a pattern that forms three groupings. The main group is formed by numerous AN fibers that preserve their relative spatial trajectory within the nucleus as they progress posteriorly and topographically through the posteroventral CN (PVCN) and into the DCN (Muniak et al., 2013). A second group of fibers courses ventromedially from the injection site and can be followed to enter the trapezoid body. The third, relatively small group of fibers rises dorsally as it passes caudally through the ventral CN (VCN). This smaller bundle corresponds to the tuberculoventral tract described by Lorente de Nó (1981). Its trajectory crosses with AN fibers at the VCN–DCN junction and can be followed to its origin in the DCN (Fig. 2).

Retrogradely labeled cells were identified in the DCN following each AVCN injection (Fig. 3). The cells were limited to the deep layers of the DCN and were dispersed throughout its depth. Labeled cell bodies appear flecked with fluorescent tracer, exhibiting a variable number of primary dendritic stalks (and possibly the axon; Fig. 3D,E). Our retrograde fills were insufficient to reveal the full dendritic arborization of each neuron, so morphological characterizations had to be based primarily on the soma and primary processes. Cell bodies appear slightly elongated but are quite variable in shape. Somatic diameters fall within the range of 10–25 μm. Each cell body gave rise to approximately one to four primary dendrites that were often oriented

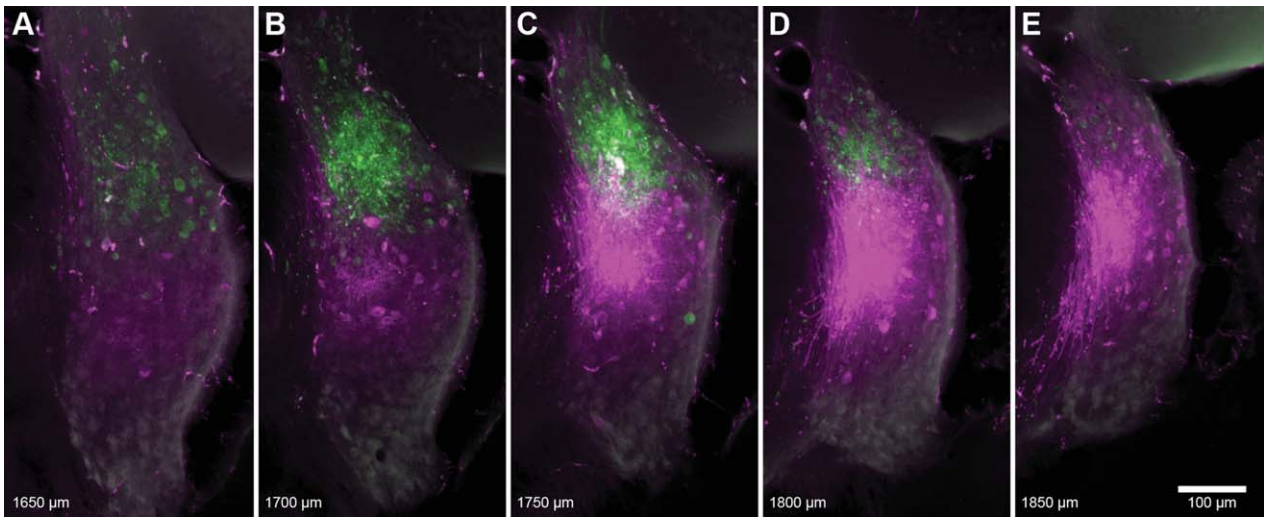

Figure 1. Fluorescent photomicrographs of serial coronal sections, 50-μm-thick, spanning a pair of injection sites (38-Rhod/Fluo, Table 1). Both rhodamine (magenta, 10.0 kHz BF) and fluorescein (green, 17.7 kHz BF) injections were located in the AVCN. Values at bottom left designate relative distance from the posterior pole of the CN. The location of the fluorescein injection is both more dorsal and posterior to that of the rhodamine injection. Faint strands of labeled AN fibers can be found ventral to each injection. Larger fibers ventromedial to the rhodamine injection can be seen entering the trapezoid body. Scale bar = 100 μm.

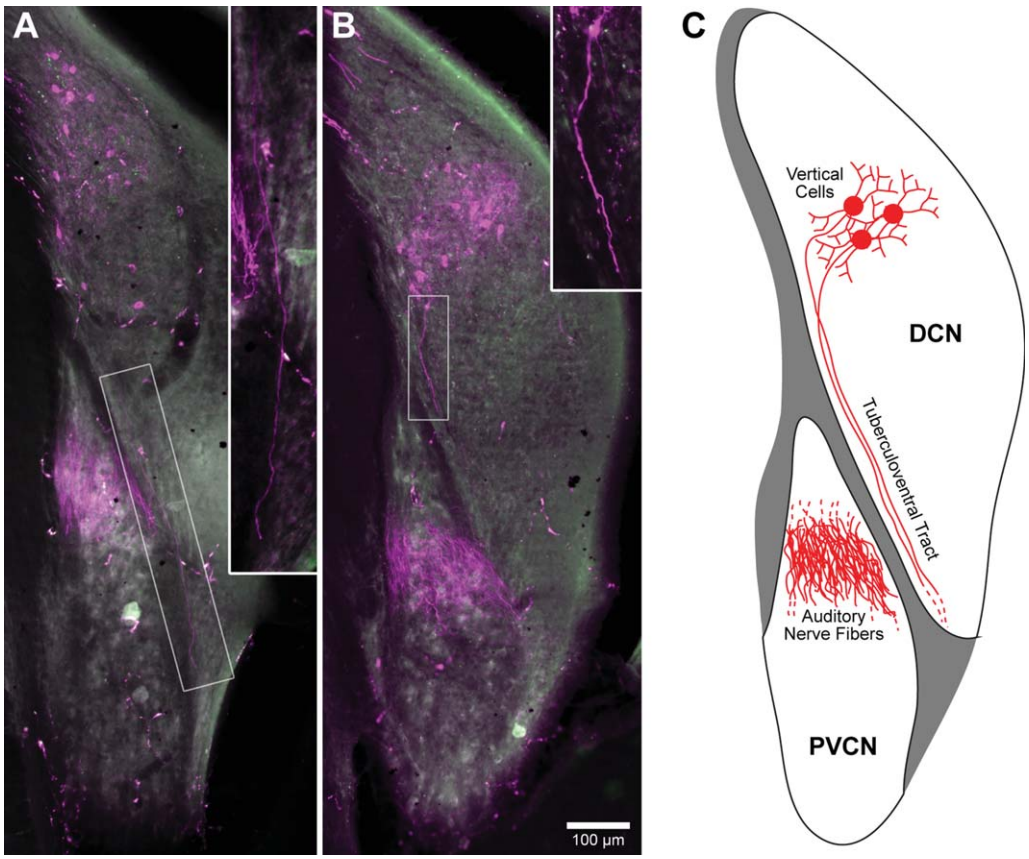

Figure 2. Fluorescent photomicrographs of coronal sections showing labeled fibers of the tuberculoventral tract in two separate animals. **A:** Fibers belonging to the descending branch of the AN were labeled by rhodamine (magenta, 33.7 kHz BF; 31-Rhod, Table 1) and are found in the dorsal region of the PVCN. Additionally, labeled vertical cells are located in the dorsomedial region of the DCN. A single labeled axon of the tuberculoventral tract (**inset**) is seen coursing ventrolaterally along the border between the PVCN and DCN and is distinct from the bundle of AN fibers. **B:** AN fibers and vertical cells have been labeled by rhodamine (magenta, 25.0 kHz BF; 33-Rhod, Table 1). Part of an axon of the tuberculoventral tract is indicated (**inset**). **C:** Schematic drawing illustrating the relative position of labeled AN fibers, vertical cells, and their axons of the tuberculoventral tract. Tuberculoventral axons can be readily distinguished from the bundle of AN fibers by their location and trajectory. Scale bar = 100 μm.

toward the pial surface of the nucleus. For each cell, the collective dendritic arborization formed a "spatial envelope" that conformed to an isofrequency sheet defined by the incoming auditory nerve fibers. Shorter dendritic branches extended in other directions as well but were largely confined to the planar sheet that also contained the labeled cell body. These features were consistent with previous morphological descriptions of vertical cells (Lorente de Nó, 1981; Webster and Trune, 1982; Saint Marie et al., 1991; Zhang and Oertel, 1993; Rhode, 1999).

Each injection produced from 11 to 128 labeled vertical cells (mean 48.4 ± 33.1 cells; Table 1). In each instance, labeled elements were concentrated within a restricted region of the DCN, forming a distinct group (Fig. 3A–C). When these sections were aligned and placed in serial order, the separate groupings of cells collectively formed discrete "sheets" along the anterior–posterior axis.

We visualized the arrangement of labeled cells within a 3D CN model by normalizing their positions according to their computed transformation matrices (Fig. 4, Supp. Info. Video 1; see Materials and Methods). Grouped by injection, cells from any single case were clearly restricted to just a portion of the DCN. Cell groups from paired injections were easily distinguished from one another, with cells matched to higher BFs situated more toward the dorsoposterior tip of the DCN. The Euclidian distance between cells from any particular group ranged from 7.6 to 535.6 μm (mean 168.5 ± 83.4 μm; 43,555 unique pairs). The majority of this variation in distance lay within the imaginary "sheet" or plane occupied by each cell group. Far less physical separation of cells was observed orthogonal to this plane. The trajectory of this plane is quite similar to the path taken by descending AN fibers as they terminate within the deep layers of the DCN (Muniak et al.,

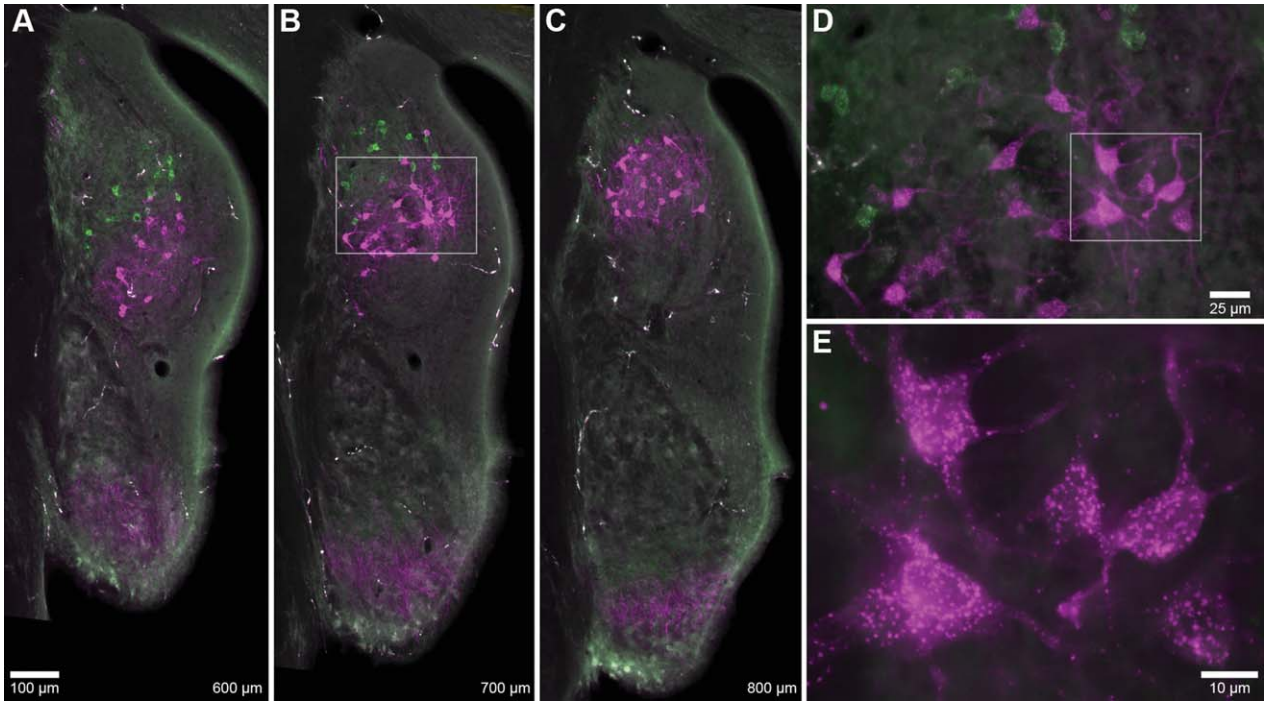

Figure 3. Photomicrographs of labeled vertical cells. **A–C:** Coronal sections through the DCN and PVCN spaced 100 µm apart. AN fibers and vertical cells were labeled by the pair of injections shown in Figure 1 (38-Rhod/Fluo, Table 1). Vertical cells (and faint AN fibers) matched to the higher BF injection (green, 17.7 kHz; magenta, 10.0 kHz) are consistently located more posterodorsally. Cells are distributed throughout the deep layers of the DCN and do not occupy superficial layers. Values at bottom right designate relative distance from the posterior pole of the CN. **D:** High magnification of vertical cells from the boxed area in B. The longer branches of vertical cell dendrites tended to extend toward the superficial layers (upper right). **E:** High magnification of vertical cells from the boxed area in D. Cell bodies were slightly elongated and variable in shape, consistent with previous descriptions of vertical cells (Zhang and Oertel, 1993; Rhode, 1999). Scale bars = 100 µm in A (applies to A–C); 25 µm in D; 10 µm in E.

2013). In cases in which AN fibers were also labeled, primary afferents and vertical cells were independently found to occupy the same area of the DCN (Fig. 4, Supp. Info. Video 1).

Tonotopic arrangement of vertical cells

We explored the relationship between vertical cell location and frequency tuning by normalizing the coordinates of all 1,259 cells in our data set within the 3D DCN model, shading each point with respect to the BF of its paired injection site (Fig. 5A, Supp. Info. Video 1). A conspicuous frequency organization emerged: "cool" blue hues (low BF) gradually transition to "warm" red hues (high BF) along an approximate anteroventral–posterodorsal axis. This relationship indicated that cells labeled by injections with the lowest BFs were distributed in the most anteroventral region of the DCN, whereas cells matched to high frequencies were restricted to the posterodorsal regions. Low-BF injections tended to label more vertical cells than high-BF injections (Fig. 5B; $R^2 = 0.32$, $P < 0.003$), though the reason for this tonotopic feature is unclear.

We considered the possibility that the variation in vertical cell counts might relate to injection size, and hence the relative uptake zone for neural tracer. Visual inspection of injections suggested no obvious link, with some of the largest apparent cases producing relatively low cell counts. Quantifying the size of an injection site is notoriously difficult because of the ambiguity in determining the edge of the effective uptake region. Furthermore, the apparent size of a fluorescent injection site is subject to the effects of photobleaching and exposure time when collecting images. Despite these caveats, a preliminary attempt to estimate injection size indicated little correlation with numbers of labeled vertical cells (Muniak, 2011). Another approach to the question that did not require injection quantification was to compare cell counts with other neural elements labeled by the injections, such as AN fibers that can be traced back to their cochlear origins (Muniak et al., 2013). If injection size covaries with tracer uptake, then one might expect a larger injection to produce both higher cell counts and broader labeling in the cochlea. There was a poor relationship, however, between these

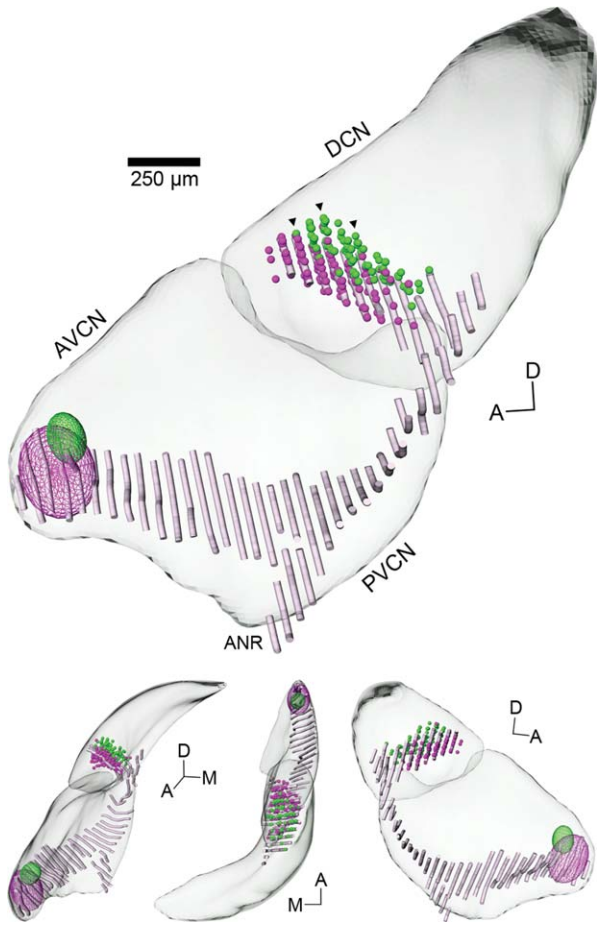

Figure 4. 3D reconstruction of cochlear nucleus illustrating locations of labeled vertical cells and AN fibers. Labeled data from all sections belonging to the case shown in Figures 1 and 3 (38-Rhod/Fluo, Table 1) were normalized to a 3D template of the CN. Small spheres were used to indicate the positions of vertical cells in the DCN labeled by rhodamine (magenta) or fluorescein (green) injections in the AVCN. Wireframe ellipsoids were used to approximate the locations of each injection shown in Figure 1. Black arrowheads indicate the position of sections shown in Figure 3. Pale magenta "noodles" represent the 3D trajectory of AN fibers labeled by the rhodamine injection (data taken from Muniak et al., 2013). A systematic relationship can be seen between the relative locations of injection sites, projection patterns of AN fibers, and vertical cells. The top figure is from a medial viewpoint. Lower figures are from alternate viewing angles; L-R: anterior, dorsal, and lateral. Abbreviations: A, anterior; ANR, auditory nerve root; D, dorsal; M, medial. Scale bar = 250 μm for large figure only.

parameters ($R = 0.34$, $P = 0.092$; see "Spread %" in Table 2 from Muniak et al., 2013), suggesting that our counts were not significantly skewed by variations in injection size.

Previous descriptions of vertical cells have noted their confinement to the deep layers of the DCN. We corroborated this finding by creating a 3D surface of the deep layer (Fig. 5A), following the same method (and source data) used to create the VCN and DCN surfaces (Muniak et al., 2013). The majority of cells were confined within the deep layer. This determination is notable given the fact that the surface and cells originated from independent sources of data, each separately normalized to the 3D template. Only 11.8% of the labeled cells (148/1,259) were located outside the boundary of the deep layers, separated by an average distance of 15.3 ± 11.4 μm (Fig. 5C). However, 98% (145/148) of these external cells still remained within 40 μm of the surface boundary.

We used various methods to evaluate quantitatively the tonotopic organization of vertical cells. First, we performed principal component analysis on the normalized data set and visualized the axis of the first principal component in three (spatial) dimensions, allowing it to pass through the Euclidian center of mass of the data set (Fig. 5A, black line). Not surprisingly, this axis was oriented toward the posterodorsomedial corner of the DCN. The first principal component accounted for 75% of the variance in the data set (Fig. 5D), indicating that vertical cells are largely organized along one dimension in the DCN with respect to frequency.

A second method for quantitatively assessing tonotopic organization was to perform multiple regression analysis (MRA) on the normalized data set. The data set was best fit by a linear equation:

$$\log_{10} f = 194.749 - 0.023M - 0.092D - 0.077P$$

where f is the BF in kilohertz, M is the medial–lateral coordinate (in micrometers) within the reference frame of our 3D CN template (low values are medial), D is the dorsal–ventral coordinate (low values are dorsal), and P is the anterior–posterior coordinate (low values are posterior). This equation produced a strong and significant correlation between BF and spatial position ($R^2 = 0.87$, $P < 0.0001$). The regression function axis was visualized as described above, passing through the center of mass (Fig. 5A, gray line). Resembling the first principal component axis, there was a strong posterodorsal orientation. As reflected in the equation, however, there was less weighting in the medial direction.

MRA predictions were compared with measured BF values by calculating the difference error in octaves (Fig. 6). Error measurements ranged from −0.94 to 1.28 oct. (0.00 ± 0.30 oct.), with the bulk of values falling within a one-oct. range. There was no significance in the value ($R^2 = 0.13$, $P < 0.0001$) or magnitude ($R^2 < 0.01$, $P = 0.04$) of error values along the measured tonotopic axis. These results further support the presence of a single tonotopic axis for vertical cells in the DCN.

We also compared the difference in measured BFs as a function of Euclidian distance between pairs of

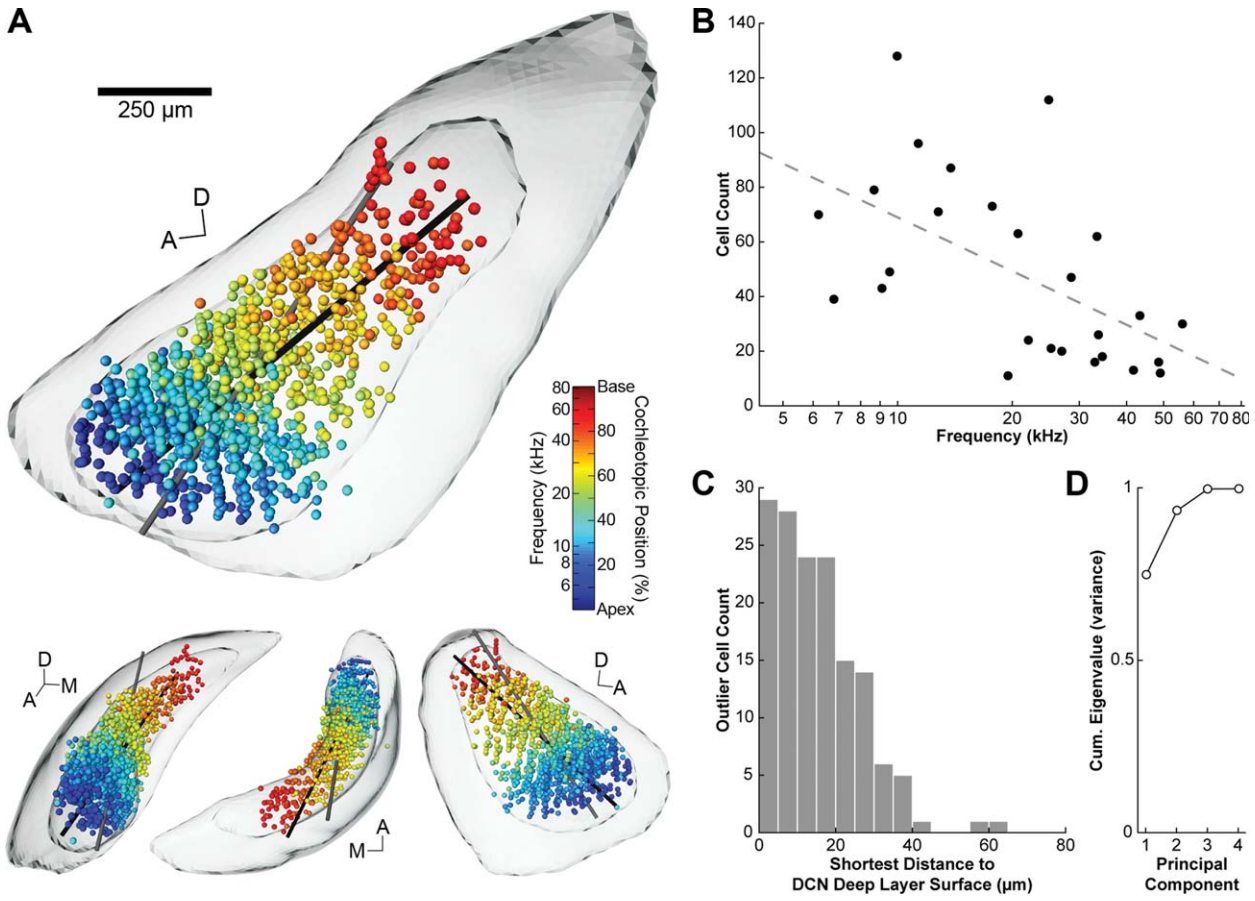

Figure 5. 3D tonotopic arrangement of vertical cells in the DCN. **A:** The normalized locations of all vertical cells in the data set are shown within the 3D model DCN. Each cell/sphere is shaded according to the BF of its paired injection site. Equivalent cochleotopic values are provided based on our frequency map (Muniak et al., 2013). Vertical cells are restricted to the confines of the deep layers (smaller surface within DCN surface) and are spatially organized with respect to BF. Black line represents the axis of the first principal component (see text). Gray line represents the axis of the multiple regression function. Both lines pass through the center of mass of the data set. The top figure is from a medial viewpoint. Lower figures are from alternate viewing angles; L-R: anterior, dorsal, and lateral. Abbreviations: A, anterior; D, dorsal; M, medial. **B:** Plot of number of vertical cells labeled by each injection as a function of injection BF. Injections with lower BFs tended to produce greater numbers of vertical cells. A regression line was fit to the data ($R^2 = 0.32$, $P < 0.003$). **C:** Histogram of shortest distances to the surface of the deep layer of the DCN for each labeled cell located outside the hull of this surface. Most cells were contained within the deep layer, and all but three of the outliers remained within 40 µm of the surface boundary. **D:** Plot of cumulative eigenvalues from principal component analysis performed on the dataset. The first principal component accounted for 75% of the variance in the distribution of labeled cells. Scale bar = 250 µm for large figure only.

vertical cells in our data set. Comparisons were made only between cells belonging to different injection groups. The number of comparisons was quite high (n = 748,356 pairs), so a density plot was used to visualize the results rather than discrete points (Fig. 7). Cells further separated in space tended to have greater differences in measured BF, although the relationship was moderate ($R^2 = 0.64$, $P < 0.0001$). This result was anticipated, because two cells with nearby BFs might lie at opposite ends of adjacent frequency planes, thus separating them by a few hundred micrometers. A similar result had been observed with comparisons between cells labeled by the same injection. Nonetheless, this finding supports the existence of tonotopic organization of vertical cells in the DCN.

Finally, we compared our data with a previously developed quantitative model of frequency organization in the mouse CN (Muniak et al., 2013). This model is based on the distribution of AN innervation in the CN with respect to cochlear origin and makes no assumptions about nor imposes directionality to frequency organization throughout the volume of the nucleus. BF predictions were made for each vertical cell based on its normalized location within the DCN. Difference errors between measured and model BF predictions were calculated, revealing a high degree of accuracy

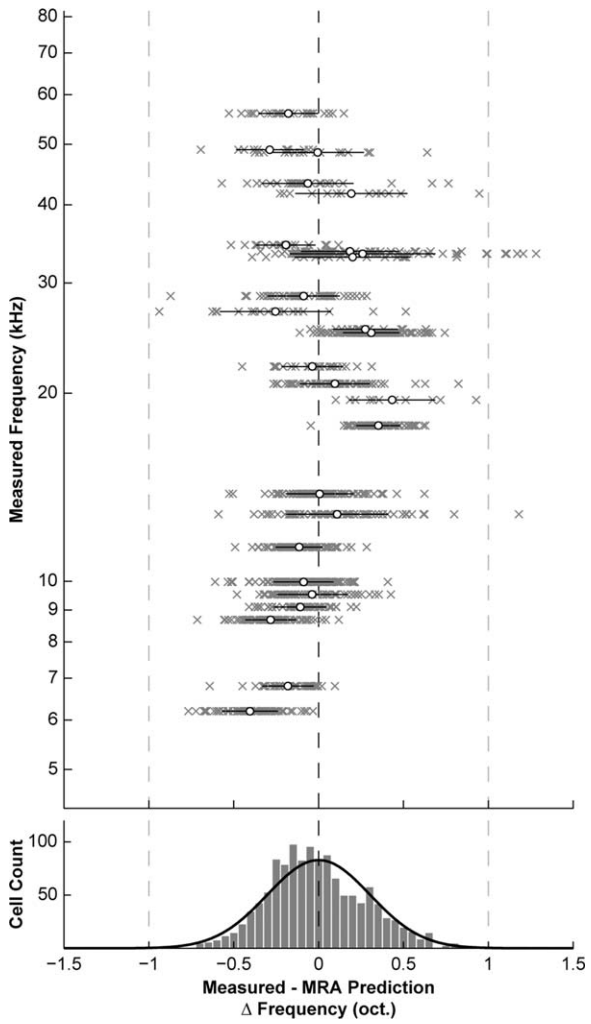

Figure 6. Prediction errors for multiple regression analysis. **Top:** Plot comparing the measured BF for each vertical cell with its predicted value according to the MRA function (see text). The axes have been swapped, and differences are plotted in octave units as a function of measured BF. All points from a single injection are grouped along a horizontal line (gray Xs). Black bars and white dots indicate mean and SD for each group. Precise matches between predicted values and measured BFs were rare, but extreme differences were scarce, and no systematic skew was observed, suggesting that the MRA function is a reasonable characterization of vertical cell location with respect to frequency. **Bottom:** Histogram summarizing distribution of prediction errors. Taken as a whole, most errors were confined to a one-octave range. A Gaussian function was fit to the distribution (0.00 ± 0.30 oct.).

(Fig. 8; $R^2 = 0.88$). Error measurements ranged from −0.82 to 1.29 oct. (0.09 ± 0.28 oct.). As with MRA predictions, the bulk of errors were within a one-oct. range, although model predictions were marginally better. In addition, there were no biases in the value ($R^2 = 0.07$, $P < 0.0001$) or magnitude ($R^2 < 0.01$, $P = 0.07$) of errors with respect to frequency. The number of positive prediction errors was greater than that of negative errors (769/1,259; 61%), and positive errors had more distal outliers, but the mean prediction error was still close to zero (Fig. 8). This result suggests that the frequency organization of vertical cells is closely matched to the tonotopic organization of primary inputs from the periphery.

To investigate further the relationship between injection size and spatial resolution of labeling, we used the frequency model to determine whether cases with larger labeled cell counts occupied broader frequency ranges in the DCN. We found a tendency for larger cell counts to have wider ranges of BF prediction errors ($R^2 = 0.21$, $P < 0.02$). However, if we considered the SD of BF prediction errors (black bars, Fig. 8, top), we found absolutely no relationship with cell counts ($R^2 = 0.0002$, $P = 0.95$). This result suggests that cases with larger numbers of labeled vertical cells do not necessarily have broader overlap with the frequency lamina of the DCN. This is notable, as frequency lamina tend to be narrower at low-frequency regions of the DCN (Muniak et al., 2013). Because low-frequency injections were more likely to produce larger cell counts, it follows that these cells must be tightly restricted to their isofrequency laminae.

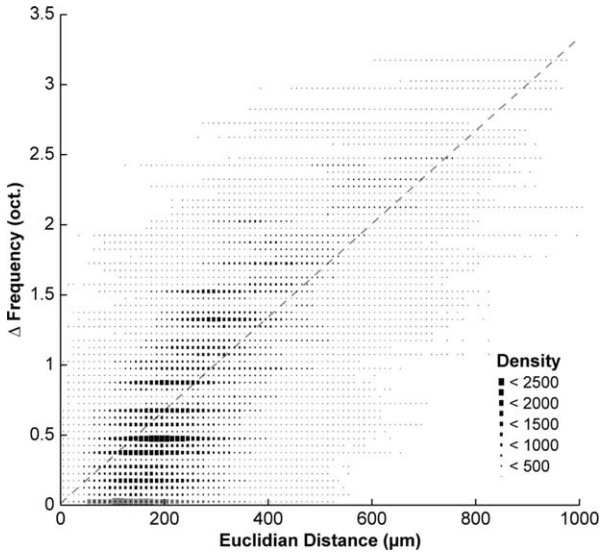

Figure 7. Density plot of the difference in measured BF values for pairs of vertical cells as a function of Euclidian distance. Differences are plotted in octave units. Bin widths are 10 μm and 0.05 oct. Bins containing larger numbers of points appear larger. Many points are scattered throughout the plot, but there is a much higher density of points along the diagonal. This indicates that the difference in vertical cell BF increases as a function of absolute distance (regression: $R^2 = 0.64$, $P < 0.0001$). Comparisons made between cells belonging to the same injection group are plotted as gray bins along the abscissa.

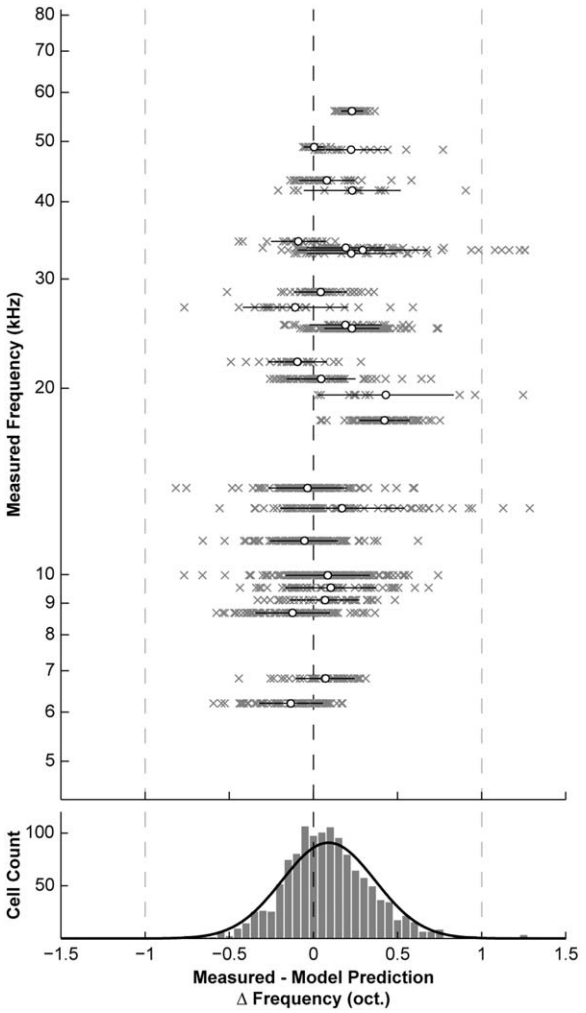

Figure 8. Prediction errors for CN frequency model. **Top:** Plot comparing the measured and predicted BFs for each vertical cell according to the CN frequency model (Muniak et al., 2013). The axes have been swapped, and differences are plotted in octave units as a function of measured BF. All points from a single injection are grouped along a horizontal line (gray Xs). Black bars and white dots indicate mean and SD for each group. Differences between measured and predicted BFs are generally small, suggesting that vertical cells are distributed with respect to the tonotopic pattern of AN input to the DCN (the basis of the model). **Bottom:** Histogram summarizing distribution of prediction errors. Most error values lie within a one-octave range. A Gaussian function was fit to the distribution (0.09 ± 0.28 oct.).

DISCUSSION

In this study, we labeled vertical cells in the DCN via physiologically targeted injections of a retrograde neuronal tracer into the AVCN. The locations of labeled cells were plotted and normalized to a 3D template of the CN, allowing us to merge data from individual cases. Various quantitative approaches converged to the same conclusion, that vertical cells are tonotopically organized within the DCN. Furthermore, this organization coincides with the input pattern of AN fibers, giving rise to a frequency-matched circuit wherein simultaneous primary AN inputs to both subdivisions of the CN are coupled by a secondary on-BF inhibitory projection from the DCN to the AVCN via the tuberculoventral tract. Key 3D concepts are presented in a summary video (Supp. Info. Video 1).

Morphological comparisons

The first comprehensive account of vertical cells was given by Lorente de Nó (1981). Studying Golgi-impregnated cell types in the tuberculum acusticum (the DCN), he described their cell bodies as being variable in size and fusiform or polygonal in shape. The cells were situated in the deep layers of the DCN; those located farther from the strial surface tended to be more likely to be seen sending axons into the tuberculoventral tract. The chief structural feature of vertical cells is the orientation of their dendritic arbors, which elaborate within a restricted plane that follows the perpendicular (vertical) axis through the laminated structure of the DCN (hence "vertical"). Later studies have confirmed these descriptions (Osen, 1983; Zhang and Oertel, 1993; Rhode, 1999; Kuo et al., 2012).

Our retrograde fills were not sufficient to label the full dendritic arborization of neurons, as reported with previous applications of retrograde markers (Saint Marie et al., 1991). The appearance of incompletely stained vertical cells, however, was consistent with those earlier descriptions (Lorente de Nó, 1981; Webster and Trune, 1982; Saint Marie et al., 1991; Zhang and Oertel, 1993; Rhode, 1999), as was their distribution throughout the deep layers of the DCN (Lorente de Nó, 1981; Webster and Trune, 1982; Saint Marie et al., 1991). Some authors have found vertical cells to be restricted to the lower half of the deep layer (Lorente de Nó, 1981; Wickesberg and Oertel, 1988), but it is possible that vertical cells had not yet finished migrating to their mature positions in their immature specimens.

Tonotopic orientation

Early studies reported that the orientation of the dendritic arbors of vertical cells was parallel to that of incoming AN fibers (Lorente de Nó, 1981). This observation was confirmed by injections in the AVCN that labeled both projecting cells in the DCN and AN fibers (Feng and Vater, 1985; Wickesberg and Oertel, 1988). Vertical cells have also been shown to receive monosynaptic excitatory input from AN fibers (Oertel and Wu, 1989; Zhang and Oertel, 1993; Rubio and Juiz, 2004). Given evidence that the pattern of AN input largely determines the BF of neurons in the CN (Bourk et al.,

1981; Fekete et al., 1984; Spirou et al., 1993; Ryugo and May, 1993), it is reasonable to conclude that the arrangement of vertical cell BFs would follow suit. We did note that high-BF injections tended to produce slightly greater numbers of cells in lower frequency regions within the model. This result, however, likely is due to the labeling of axons of passage: the trajectory of low-BF vertical cell axons passes through high-frequency regions in the AVCN (Cao et al., 2008).

Our results demonstrate that vertical cells are arranged tonotopically and send projections to matched frequency regions of the AVCN. When the locations of labeled vertical cells were normalized in 3D, we quantitatively confirmed that their arrangement was highly organized. Cells labeled by AVCN injections at low frequencies were located more anteroventrally in the DCN, whereas those labeled by injections at progressively higher frequencies were located progressively more posterodorsally. Furthermore, comparisons with a frequency model of the CN (Muniak et al., 2013) demonstrated that the BF of each cell, inferred from the AVCN recording site, closely matched that of AN input.

Functional implications

Vertical cells are thought to be the source of type II responses in the DCN, categorized by their narrowly tuned responses to tones, low spontaneous activity, nonmonotonic rate-level functions, inhibitory sidebands, and weak responses to broadband noise (Evans and Nelson, 1973; Young and Brownell, 1976; Young and Voigt, 1982; Davis et al., 1996; Spirou et al., 1999; Rhode, 1999). Type II units can be antidromically driven from the VCN, but not by stimulation of fibers in the dorsal acoustic stria (Young, 1980). These results imply that neurons with type II characteristics project within, but not out of, the CN, consistent with anatomical reports that vertical cells lack ascending projections but do send local axons to the VCN (Lorente de Nó, 1981). Definitive evidence comes from intracellular recordings and fills of neurons producing type II responses, which reveal cells matching the morphological descriptions of vertical cells (Rhode, 1999).

The tonotopic organization of vertical cells is consistent with the cochleotopic projections of the AN into the DCN (Ryugo and May, 1993; Muniak et al., 2013), the presence of AN synapses onto their dendrites (Rubio and Juiz, 2004), and excitatory synaptic inputs from auditory nerve fibers (Kuo et al., 2012). The result would be a tonotopic projection to AVCN neurons that are matched in BF (Wickesberg and Oertel, 1988; Muniak et al., 2013). This conclusion is consistent with reports of on-BF inhibition of bushy and stellate cells in the AVCN (Wickesberg and Oertel, 1990), in which the blocking of inhibitory amino acid inputs to the AVCN resulted in on-BF rate increases with little to no increase in off-BF spiking (Caspary et al., 1994). It has been proposed that this connection may be a disynaptic pathway for echo suppression (Wickesberg and Oertel, 1990; Wickesberg, 1996), with the timing of the inhibitory projection to the AVCN offset by the axon conduction velocity and a single synaptic delay. Recent evidence has also suggested that glycinergic inhibition is necessary to improve the temporal precision of spike timing in bushy and T-stellate cells, albeit on different time scales, in order to refine the encoding of the fine structure and envelope cues, respectively, of the acoustic signal (Xie and Manis, 2013). This local circuit between the DCN and the VCN might, therefore, be one mechanism for enhancing the fidelity of CN output.

Type II units are considered the source of near-BF narrowband inhibition on type IV responses (Voigt and Young, 1980, 1990). This inhibition helps to shape the spectral tuning of DCN principal cells (Nelken and Young, 1994; Spirou et al., 1999; Davis and Young, 2000). Recent work has shown functional synapses from vertical cells to pyramidal cells within *in vitro* slices (Kuo et al., 2012). The tonotopic distribution of vertical cells demonstrated in the present study fits well with this picture, and the 3D grouping of cells associated with the same BF affirms the idea that cell types united by a common frequency in the DCN are organized into slabs (Spirou et al., 1993). Reconstructed axons of at least some vertical cells are constrained in sheets, much like their dendrites (Rhode, 1999). Thus, the near-BF inhibition of type IV units (pyramidal cells) by type II units is a result of the local ramification of vertical cell axons within an isofrequency slab. Such inhibition patterns emerge from either narrowband stimuli or spectral notches, i.e., in narrow frequency variations of an ongoing sound. Because many natural sounds, including communication signals, are characterized by distinct, time-varying changes in their spectral peaks, the type II–type IV circuitry could facilitate the detection of spectral features embedded within these sounds (Nelken and Young, 1996). Overall, these results suggest that vertical cells provide rapid on- or near-BF inhibition to cells of both the DCN and the AVCN, although more data are needed to understand the function of these neurons better.

Our results suggest that there are greater absolute numbers of low-BF vertical cells than high-BF cells. This observation is not easily explained by injection size in the AVCN; we found a poor relationship between the degree of labeling in the cochlea (Muniak et al., 2013) and vertical cell counts. If anything, one might expect high-BF injections to produce more cells because of

contamination of projecting axons from low-BF vertical cells. Another explanation might be the physical expansion of the low-frequency end of the DCN. In this region, the deep layer is thicker, allowing more room for vertical cells to proliferate. However, despite this change in shape, our frequency model (Muniak et al., 2013) posits roughly equal proportions of DCN volume per cochlear segment. Hence, if vertical cells are evenly distributed across frequencies, we should not see a change in absolute counts, although the 3D arrangement of these cells would shift from sheets to clusters along the frequency axis. Instead, we observed both types of change in our data.

If our uneven vertical cell counts reflect normal DCN organization, how might this be explained functionally? Recent work showed that the output of a single vertical cell onto a pyramidal cell is relatively weak and that the coordination of multiple vertical cells may be needed to inhibit principal cell spiking (Kuo et al., 2012). There is a tendency for type II units to have lower BFs than the type IV units that they are suppressing (Voigt and Young, 1990), a trend also seen when glycinergic neurotransmission is blocked (Davis and Young, 2000); this result is not surprising given the low-frequency tails of AN tuning curves (Kiang and Moxon, 1974). The addition of more vertical cells could be one way to adapt to greater functional demands at the low end of the frequency spectrum, but other probable adaptive scenarios include revised innervation patterns and/or modifications to pre- and postsynaptic machinery.

An alternative, though not mutually exclusive, possibility for the tonotopic variation in cell counts arises from a hypothesized role of vertical cell projections to the VCN. The tuberculoventral projection might reduce or reverse the effects of spectral changes to complex sounds caused by the acoustical transfer function of the pinnae (Rice et al., 1992; Nelken and Young, 1996). In this scenario, vertical cells may weakly inhibit VCN neurons outside the range of spectral notches in order to "rebalance" the sound field to its original spectral shape. With the mouse ear, spectral notches are observed largely in the >20-kHz range (Lauer et al., 2011), which is where our vertical cell counts are the lowest. Furthermore, the transfer function of the mouse ear shows overall gains in the 10–20-kHz range (Lauer et al., 2011), where our cell counts are higher. Hence, the distribution of vertical cell numbers might relate to the overall inhibitory requirements in the CN with respect to frequency.

ACKNOWLEDGMENTS

The data in the present report have not been previously published but did originate from tissue used in a study of AN organization in the cochlea and cochlear nucleus (Muniak et al., 2013). We thank Karen Montey, Alejandro Rivas, Brad May, and Howard Francis who participated in the original experiments. Some of the data were included as part of a dissertation submitted in partial fulfillment of a PhD degree in Neuroscience to the Johns Hopkins University (Muniak, 2011).

CONFLICT OF INTEREST STATEMENT

The authors have no conflicts of interest to report.

ROLE OF AUTHORS

Both authors had full access to all the data in the study and take responsibility for the integrity of the data and the accuracy of data analysis. Study concept and design: MAM, DKR. Data acquisition, analyses, and interpretation: MAM with guidance from DKR. Drafting of the manuscript: MAM, DKR.

LITERATURE CITED

Bourk TR, Mielcarz JP, Norris BE. 1981. Tonotopic organization of the anteroventral cochlear nucleus of the cat. Hear Res 4:215–241.

Brawer JR, Morest DK, Kane EC. 1974. The neuronal architecture of the cochlear nucleus of the cat. J Comp Neurol 155:251–300.

Burian M, Gstoettner W. 1988. Projection of primary vestibular afferent fibers to the cochlear nucleus in the guinea pig. Neurosci Lett 84:13–17.

Caicedo A, Herbert H. 1993. Topography of descending projections from the inferior colliculus to auditory brainstem nuclei in the rat. J Comp Neurol 328:377–392.

Cao XJ, McGinley MJ, Oertel D. 2008. Connections and synaptic function in the posteroventral cochlear nucleus of deaf jerker mice. J Comp Neurol 510:297–308.

Caspary DM, Backoff PM, Finlayson PG, Palombi PS. 1994. Inhibitory inputs modulate discharge rate within frequency receptive fields of anteroventral cochlear nucleus neurons. J Neurophysiol 72:2124–2133.

Davis KA, Young ED. 2000. Pharmacological evidence of inhibitory and disinhibitory neuronal circuits in dorsal cochlear nucleus. J Neurophysiol 83:926–940.

Davis KA, Ding J, Benson TE, Voigt HF. 1996. Response properties of units in the dorsal cochlear nucleus of unanesthetized decerebrate gerbil. J Neurophysiol 75:1411–1431.

Evans EF, Nelson PG. 1973. The responses of single neurones in the cochlear nucleus of the cat as a function of their location and the anaesthetic state. Exp Brain Res 17: 402–427.

Fekete DM, Rouiller EM, Liberman MC, Ryugo DK. 1984. The central projections of intracellularly labeled auditory nerve fibers in cats. J Comp Neurol 229:432–450.

Feng AS, Vater M. 1985. Functional organization of the cochlear nucleus of rufous horseshoe bats (*Rhinolophus rouxi*): frequencies and internal connections are arranged in slabs. J Comp Neurol 235:529–553.

Franklin KBJ, Paxinos G. 1997. The mouse brain in stereotaxic coordinates. San Diego: Academic Press.

Haenggeli CA, Pongstaporn T, Doucet JR, Ryugo DK. 2005. Projections from the spinal trigeminal nucleus to the cochlear nucleus in the rat. J Comp Neurol 484:191–205.

Itoh K, Kamiya H, Mitani A, Yasui Y, Takada M, Mizuno N. 1987. Direct projections from the dorsal column nuclei and the spinal trigeminal nuclei to the cochlear nuclei in the cat. Brain Res 400:145–150.

Kanold PO, Young ED. 2001. Proprioceptive information from the pinna provides somatosensory input to cat dorsal cochlear nucleus. J Neurosci 21:7848–7858.

Kiang NY, Moxon EC. 1974. Tails of tuning curves of auditory-nerve fibers. J Acoust Soc Am 55:620–630.

Kuo SP, Lu HW, Trussell LO. 2012. Intrinsic and synaptic properties of vertical cells of the mouse dorsal cochlear nucleus. J Neurophysiol 108:1186–1198.

Lauer AM, Slee SJ, May BJ. 2011. Acoustic basis of directional acuity in laboratory mice. J Assoc Res Otolaryngol 12: 633–645.

Lorente de Nó R. 1981. The primary acoustic nuclei. New York: Raven Press.

Ma WL, Brenowitz SD. 2012. Single-neuron recordings from unanesthetized mouse dorsal cochlear nucleus. J Neurophysiol 107:824–835.

Malmierca MS, Le Beau FE, Rees A. 1996. The topographical organization of descending projections from the central nucleus of the inferior colliculus in guinea pig. Hear Res 93:167–180.

Malmierca MS, Merchan MA, Henkel CK, Oliver DL. 2002. Direct projections from cochlear nuclear complex to auditory thalamus in the rat. J Neurosci 22:10891–10897.

Meltzer NE, Ryugo DK. 2006. Projections from auditory cortex to cochlear nucleus: a comparative analysis of rat and mouse. Anat Rec A Discov Mol Cell Evol Biol 288:397–408.

Muniak MA. 2011. Anatomical and physiological bases of frequency organization in the mouse auditory brainstem. Baltimore: Johns Hopkins University.

Muniak MA, Rivas A, Montey KL, May BJ, Francis HW, Ryugo DK. 2013. 3D model of frequency representation in the cochlear nucleus of the CBA/J mouse. J Comp Neurol 521:1510–1532.

Nelken I, Young ED. 1994. Two separate inhibitory mechanisms shape the responses of dorsal cochlear nucleus type IV units to narrowband and wideband stimuli. J Neurophysiol 71:2446–2462.

Nelken I, Young ED. 1996. Why do cats need a dorsal cochlear nucleus? J Basic Clin Physiol Pharmacol 7:199–220.

Oertel D, Wu SH. 1989. Morphology and physiology of cells in slice preparations of the dorsal cochlear nucleus of mice. J Comp Neurol 283:228–247.

Ohlrogge M, Doucet JR, Ryugo DK. 2001. Projections of the pontine nuclei to the cochlear nucleus in rats. J Comp Neurol 436:290–303.

Osen KK. 1969. Cytoarchitecture of the cochlear nuclei in the cat. J Comp Neurol 136:453–484.

Osen KK. 1972. Projection of the cochlear nuclei on the inferior colliculus in the cat. J Comp Neurol 144:355–372.

Osen KK. 1983. Orientation of dendritic arbors studied in Golgi sections of the cat dorsal cochlear nucleus. In: Webster WR, Aitkin LM, editors. Mechanisms of hearing. Clayton, Australia: Monash University Press. p 83–89.

Rhode WS. 1999. Vertical cell responses to sound in cat dorsal cochlear nucleus. J Neurophysiol 82:1019–1032.

Rice JJ, May BJ, Spirou GA, Young ED. 1992. Pinna-based spectral cues for sound localization in cat. Hear Res 58: 132–152.

Rubio ME, Juiz JM. 2004. Differential distribution of synaptic endings containing glutamate, glycine, and GABA in the rat dorsal cochlear nucleus. J Comp Neurol 477:253–272.

Ryugo DK, May SK. 1993. The projections of intracellularly labeled auditory nerve fibers to the dorsal cochlear nucleus of cats. J Comp Neurol 329:20–35.

Ryugo DK, Willard FH, Fekete DM. 1981. Differential afferent projections to the inferior colliculus from the cochlear nucleus in the albino mouse. Brain Res 210:342–349.

Saint Marie RL, Benson CG, Ostapoff EM, Morest DK. 1991. Glycine immunoreactive projections from the dorsal to the anteroventral cochlear nucleus. Hear Res 51:11–28.

Spirou GA, May BJ, Wright DD, Ryugo DK. 1993. Frequency organization of the dorsal cochlear nucleus in cats. J Comp Neurol 329:36–52.

Spirou GA, Davis KA, Nelken I, Young ED. 1999. Spectral integration by type II interneurons in dorsal cochlear nucleus. J Neurophysiol 82:648–663.

Voigt HF, Young ED. 1980. Evidence of inhibitory interactions between neurons in dorsal cochlear nucleus. J Neurophysiol 44:76–96.

Voigt HF, Young ED. 1990. Cross-correlation analysis of inhibitory interactions in dorsal cochlear nucleus. J Neurophysiol 64:1590–1610.

Webster DB, Trune DR. 1982. Cochlear nuclear complex of mice. Am J Anat 163:103–130.

Weedman DL, Ryugo DK. 1996. Pyramidal cells in primary auditory cortex project to cochlear nucleus in rat. Brain Res 706:97–102.

Weinberg RJ, Rustioni A. 1987. A cuneocochlear pathway in the rat. Neuroscience 20:209–219.

Wenthold RJ. 1987. Evidence for a glycinergic pathway connecting the two cochlear nuclei: an immunocytochemical and retrograde transport study. Brain Res 415:183–187.

Wickesberg RE. 1996. Rapid inhibition in the cochlear nuclear complex of the chinchilla. J Acoust Soc Am 100:1691–1702.

Wickesberg RE, Oertel D. 1988. Tonotopic projection from the dorsal to the anteroventral cochlear nucleus of mice. J Comp Neurol 268:389–399.

Wickesberg RE, Oertel D. 1990. Delayed, frequency-specific inhibition in the cochlear nuclei of mice: a mechanism for monaural echo suppression. J Neurosci 10:1762–1768.

Wickesberg RE, Whitlon D, Oertel D. 1994. In vitro modulation of somatic glycine-like immunoreactivity in presumed glycinergic neurons. J Comp Neurol 339:311–327.

Wright DD, Ryugo DK. 1996. Mossy fiber projections from the cuneate nucleus to the cochlear nucleus in the rat. J Comp Neurol 365:159–172.

Xie X, Manis PB. 2013. Target-specific IPSC kinetics promote temporal processing in auditory parallel pathways. J Neurosci 33:1598–1614.

Young ED. 1980. Identification of response properties of ascending axons from dorsal cochlear nucleus. Brain Res 200:23–37.

Young ED, Brownell WE. 1976. Responses to tones and noise of single cells in dorsal cochlear nucleus of unanesthetized cats. J Neurophysiol 39:282–300.

Young ED, Oertel D. 2003. The cochlear nucleus. In: Shepherd GM, editor. The synaptic organization of the brain, 5th ed. New York: Oxford University Press. p 125–163.

Young ED, Voigt HF. 1982. Response properties of type II and type III units in dorsal cochlear nucleus. Hear Res 6: 153–169.

Young ED, Nelken I, Conley RA. 1995. Somatosensory effects on neurons in dorsal cochlear nucleus. J Neurophysiol 73:743–765.

Zhan X, Ryugo DK. 2007. Projections of the lateral reticular nucleus to the cochlear nucleus in rats. J Comp Neurol 504:583–598.

Zhang S, Oertel D. 1993. Tuberculoventral cells of the dorsal cochlear nucleus of mice: intracellular recordings in slices. J Neurophysiol 69:1409–1421.